NANO LETTERS

2009
Vol. 9, No. 9
3234-3238

Charge Sensing and Controllable Tunnel Coupling in a Si/SiGe Double Quantum Dot

C. B. Simmons,* Madhu Thalakulam, B. M. Rosemeyer, B. J. Van Bael, E. K. Sackmann, D. E. Savage, M. G. Lagally, R. Joynt, Mark Friesen, S. N. Coppersmith, and M. A. Eriksson*

University of Wisconsin—Madison, Madison, Wisconsin 53706

Received May 11, 2009; Revised Manuscript Received July 16, 2009

ABSTRACT

We report integrated charge sensing measurements on a Si/SiGe double quantum dot. The quantum dot is shown to be tunable from a single, large dot to a well-isolated double dot. Charge sensing measurements enable the extraction of the tunnel coupling *t* between the quantum dots as a function of the voltage on the top gates defining the device. Control of the voltage on a single such gate tunes the barrier separating the two dots. The measured tunnel coupling is an exponential function of the gate voltage. The ability to control *t* is an important step toward controlling spin qubits in silicon quantum dots.

Following a proposal to use gated quantum dots to host spin qubits in semiconductors,[1] a series of recent experiments using GaAs/AlGaAs heterostructures have demonstrated the measurement and manipulation of quantum dot semiconductor spin qubits.[2−8] At low temperatures, the T_2 dephasing time for semiconductor spin qubits is usually limited by hyperfine coupling between the electron and nuclear spins.[9−11] Because Si and Ge have abundant isotopes with zero nuclear spin, a number of proposals for spin qubits in semiconductors have focused on these materials,[12−15] and gated quantum dots have now been fabricated in Si/SiGe,[16−20] Si-MOS systems,[21−29] Si nanowires,[30−33] and patterned donor layers.[34]

One of the important features of quantum dots is that they can be easily coupled to one another in the form of a double quantum dot. The tunnel coupling *t* between the two dots in a double dot is an important quantity, because several different qubit operations can be performed by controlling this tunnel rate as a function of time. For approaches in which the qubit is a single electron spin, control of *t* enables the performance of SWAP operations between two qubits.[1] In a two-electron triplet−singlet qubit, controlling *t* enables single-qubit rotations.[35] And in an architecture in which each logical qubit is composed of three spins in three different quantum dots, control of *t* alone enables universal quantum computation.[36]

Here we report measurements of a Si/SiGe double quantum dot with an integrated quantum point contact (QPC) used for charge sensing. The lateral confinement of the quantum dot is tuned elecrostatically using metal top gates, and the device characteristics allow comprehensive control of the interdot tunnel coupling. We demonstrate a smooth transition from a well-defined double dot with weak tunnel coupling, through a strongly coupled quantum dot molecule, to a single, large quantum dot. Charge sensing with the QPC is used to probe the transfer of charge from one dot to the other. The sharpness of this charge transition depends critically on the interdot tunnel coupling, and fits to this transition allow the tunnel coupling to be extracted over the range from a weakly to a strongly coupled double dot. We measure a change in the tunnel coupling of more than a factor of 10, corresponding to more than a 100-fold modulation in the exchange coupling between the quantum dots.

A scanning electron micrograph of the device design is shown in Figure 1a. The two-dimensional electron system (2DES) is located approximately 75 nm below the surface of the heterostructure. The carrier density and mobility of the 2DES determined from Hall and Shubnikov−de Haas measurements are 5×10^{11} cm^{-2} and 44000 cm^2/(V s), respectively. The device was measured in a dilution refrigerator with a base temperature of 25 mK and an extracted electron temperature of 182 mK (discussed in detail below). The four gates labeled *T*, *L*, *M*, and *R* are used to create the quantum dot confinement, while gate *Q*, in combination with gate *L*, forms the electrostatically coupled QPC. This device design incorporates several features that appear to be important for the results reported here. First, in order to minimize the dot size, and similar to ref 7, this device does not have the "plunger" gates that are often found in double

* Corresponding authors, cbsimmons@wisc.edu and maeriksson@wisc.edu.

10.1021/nl9014974 CCC: $40.75
Published on Web 07/31/2009

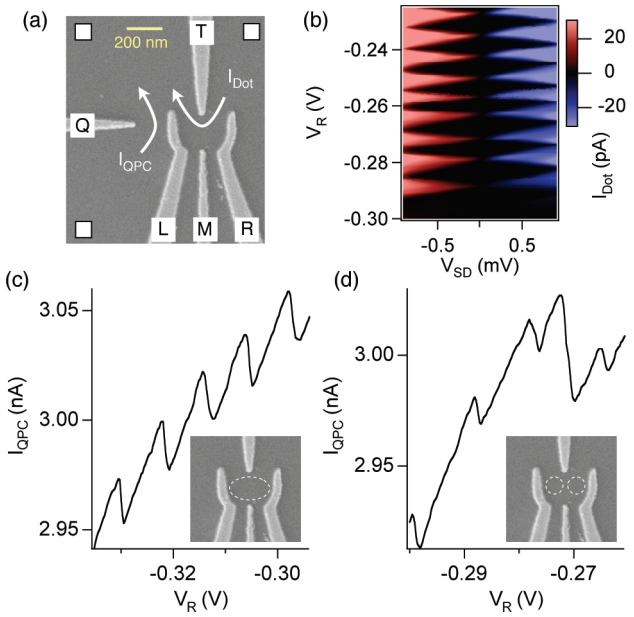

Figure 1. (a) Scanning electron micrograph showing the top gate geometry for the measured device. The transport current through the dot is indicated by I_{dot} and the charge sensor current by I_{QPC}. (b) Coulomb diamonds measured in transport through the quantum dot tuned to be a single dot. (c) Charge sensing signal from the coupled quantum point contact showing the periodic steps in I_{QPC} resulting from charge transitions on the neighboring single quantum dot, shown schematically by the dashed oval superimposed on the SEM image. (d) Charge sensing signal from a weakly coupled double dot, showing two different charge sensing amplitudes.

quantum dot designs. The result is that each side of the quantum dot is smaller than previously published Si/SiGe quantum dots that have implemented a similar gate geometry.[17,19,20] Second, the side-gates L and R are quite narrow ($\sim$ 40% the width of the side-gate in ref 20) in order to reduce the screening between the dot and the QPC to maximize the sensor response to charge transitions. As we show below, this quantum dot can be tuned to be a single or a double quantum dot by adjusting the voltage on the middle gate V_M.

In the single dot regime, with small $|V_M|$, symmetric Coulomb diamonds are observed in the transport current through the dot I_{dot} as a function of the source−drain voltage V_{SD} and V_R, as shown in Figure 1b. The last measurable diamond gives a single-dot charging energy $E_c = e^2/C =$ 880 μeV and a capacitance between gate R and the dot of 17 aF. The charging energy corresponds to a total dot capacitance $C = 182$ aF, and this gives a lever arm $C_R/C =$ 0.092. After this last diamond, the tunnel barriers between the dot and the leads are too opaque to identify further charge transitions using transport current through the dot and charge sensing must be used.

Parts c and d of Figure 1 show the use of a nearby QPC for noninvasive measurement of the charge states of the quantum dot(s). As V_R is made more negative, electrons are removed from the dot, and the resulting decrease in the electrostatic potential of the dot causes a sudden increase in I_{QPC}. In addition, there is an overall linear decrease in I_{QPC} due to the direct coupling between gate R and the QPC,

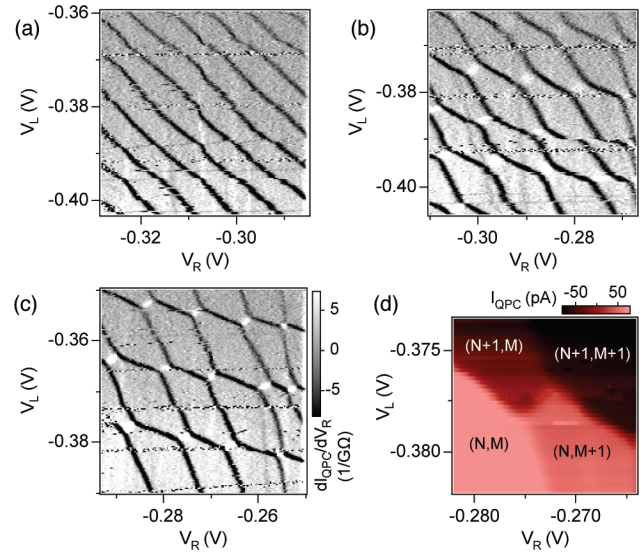

Figure 2. (a−c) dI_{QPC}/dV_R measured as a function of V_R and V_L for increasing $|V_M|$ (−0.5, −0.7, and −1.0 V) (gray scale shown in (c)). Three regimes of the quantum dot are evident from the dark transition lines: a single, large dot; a strongly coupled quantum dot molecule; and a weakly coupled double dot. (d) I_{QPC} at a single vertex of the honeycomb diagram with a background plane removed, showing four charge states of the double dot.

resulting in the sawtooth pattern of I_{QPC} vs V_R shown in Figure 1c. The uniform height and periodic steps in I_{QPC} indicate the presence of a single quantum dot. When the dot is tuned into a weakly coupled double dot, the charge sensor reports two distinct amplitudes for transitions on the left and right dots, as seen in Figure 1d. The left dot is physically closer to the QPC, and it produces a larger step $\delta I \sim 50$ pA, while a one electron change on the right dot yields $\delta I \sim 15$ pA. These charge signals on the QPC correspond to $\sim 7 \times 10^{-3}$ e^2/h and 2×10^{-3} e^2/h for the left and right dot, respectively, in good agreement with observations in similar systems.[37]

Figure 2a−c show the transition from a single dot to a well-separated double dot, as indicated by the charge sensing signal dI_{QPC}/dV_R as a function of V_R and V_L, taken at three increasingly negative values of the voltage on the middle gate V_M. The numerical differentiation of I_{QPC} as a function of V_R highlights the charge transitions on the dot which appear as black or white lines in these plots. In Figure 2a, with $V_M = -0.5$ V, the charge transitions form a single set of parallel lines, indicating that the system is composed of a single, large quantum dot. The charge transitions are nearly symmetric with respect to V_R and V_L, implying that the single quantum dot is coupled roughly equally to gate R and gate L, as expected based on the symmetric lithographic gate design (Figure 1a). By making the voltage on gate M more negative ($V_M = -0.7$ V), the single dot is split into a strongly coupled double dot, where the left side is coupled dominantly to gate L and the right side to gate R, as shown by the bending of the transition lines in Figure 2b. Further decrease V_M to −1.0 V results in the weak-coupling regime and a well-isolated pair of quantum dots (Figure 2c).

The charge transition lines in Figure 2c form the expected honeycomb pattern where each cell of the honeycomb

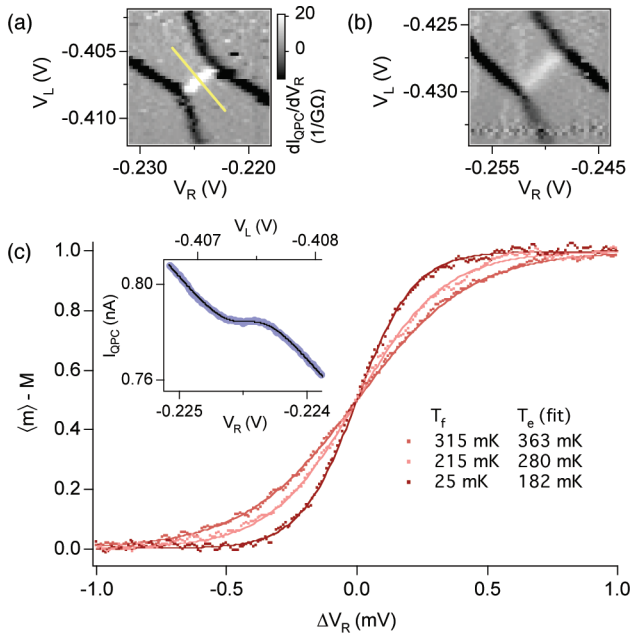

Figure 3. dI_{QPC}/dV_R measured as a function of V_R and V_L showing a single vertex of the charge stability diagram for the double quantum dot in the weak (a) and strong (b) coupling regimes (gray scale shown in (a)). The superimposed yellow line in (a) indicates the detuning diagonal for the $(N,M+1)$ and $(N+1,M)$ charge states. (c) Inset: I_{QPC} along the detuning diagonal of a weakly coupled double dot with the corresponding fit to the interdot transition given by eq 1. Main plot: The interdot transition rescaled into units of excess charge on the right dot at three different temperatures. The solid curves are fits using eq 2 with $t = 0$. Each of the data sets corresponds to an average of 15 sweeps.

corresponds to well-defined electron occupations of the left and right dots.[38] Previous observation of double dot behavior in Si/SiGe was made in a structure that was designed to be a single quantum dot. Numerical modeling has shown how double dot behavior arises in such a structure.[39] In contrast, the device studied here was designed to provide tunable control of the tunnel coupling between dots in well-identified locations. From the slopes and the spacings of the charge transition lines in Figure 2c, we find that the left dot is coupled ~2.2 times more strongly to gate L than to gate R (the more horizontal transitions), while the right dot is coupled ~2.0 times more strongly to gate R than to gate L (the more vertical transitions).

Figure 2d shows I_{QPC} at one of the vertices of the honeycomb stability diagram with a background plane removed. Four distinct values of I_{QPC} are visible, corresponding to four different charge states on the double quantum dot. Moving an electron from the left dot to the right dot results in an increase in I_{QPC}. As shown in parts a and b of Figure 3, this increase appears as a white line in a plot of dI_{QPC}/dV_R. In Figure 3a, with $V_M = -1.0$ V, the transition appears as a sharp white line, indicating a sharp interdot transition and weak tunnel coupling between the dots. In Figure 3b, $V_M = -0.825$ V and the transition appears as a broad and less intense white line, indicating strong tunnel coupling and increased charge delocalization between the dots.

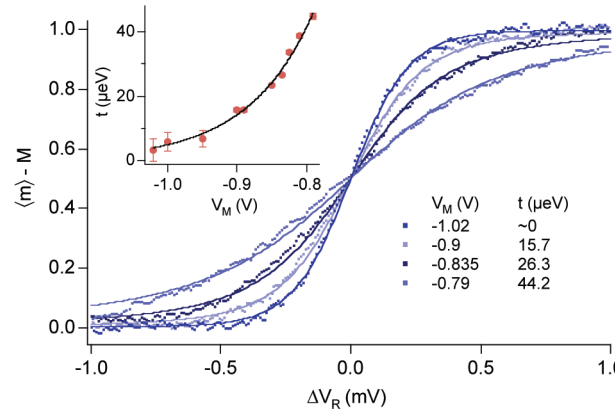

Figure 4. Excess charge on the right dot along the interdot transition taken with four different values of the double dot tunnel coupling t. Each data set is an average of 15 sweeps, and the solid lines are fits to the data using eq 2. Inset: The extracted values of t as a function of V_M. Solid line is an exponential fit to the data.

Moving along the detuning diagonal in gate voltage space, indicated by the superimposed yellow line in Figure 3a, causes a single electron to shift from one dot to the other. Measurements of this transition allow the extraction of a number of important quantities describing the double dot and the charge sensor. The inset of Figure 3c shows I_{QPC} measured as V_L and V_R are simultaneously swept to follow the detuning diagonal. On top of a linear background, due to the direct gate-QPC coupling, there is a step in I_{QPC} when $V_R \approx -0.2245$ V due to the transition between the $(N,M+1)$ and the $(N+1,M)$ charge states.

Following the method of DiCarlo et al.,[37] we treat the $(N,M+1)$ and $(N+1,M)$ charge states as a two-level system and fit the effect of the ground charge state transition on I_{QPC} using

$$I_{QPC}(\varepsilon) = I_0 + \delta I \frac{\varepsilon}{\Omega} \tanh\left(\frac{\Omega}{2k_B T_e}\right) + \frac{\partial I}{\partial \varepsilon}\varepsilon \qquad (1)$$

Here, ε is the detuning energy, T_e is the electron temperature, and Ω is the ground and excited state energy splitting, $\Omega = (\varepsilon^2 + 4t^2)^{1/2}$, where t is the tunnel coupling. I_0, δI, and $\partial I/\partial \varepsilon$ are the background current, the sensor sensitivity, and the direct gate−QPC coupling, respectively. These three parameters describe the system and are important for the extraction of the tunnel coupling below. The detuning energy ε is related to the gate voltage V_R by a lever arm α, $\varepsilon = \alpha V_R$. As shown by the solid line in the inset of Figure 3c, fits using eq 1 provide good agreement with the data. Using the results for the three fit parameters that characterize the QPC sensor, I_{QPC} can be converted into units of excess charge on the right dot, $\langle m \rangle - M$, and we report the data in the main panel of Figure 3a and in Figure 4 below in this way.

When plotted versus gate voltage, the width of the interdot charge transition is dependent on three factors: T_e, α, and t. To determine T_e and α, we tune the double dot into the weak coupling regime, where $t \approx 0$, by making V_M increasingly negative until the transition is broadened only by temperature. In this limit, and with V_M fixed, raising T_e by raising the temperature of the dilution refrigerator broadens out the

transition, as shown in Figure 3c. At low temperatures, the electron temperature is warmer than the refrigerator temperature, due to the balance between the cooling power supplied to the electron system and heating from external sources. At higher temperatures, the electron temperature T_e approaches the refrigerator temperature T_f. We fit the temperature dependence with a simple relationship between T_e and T_f, $T_e = (T_f^2 + T_0^2)^{1/2}$, where T_0 arises due to the effect of external heating. The parameters T_0 and α are determined by simultaneously fitting curves of the interdot transition in the weak coupling limit ($t = 0$ and $\varepsilon = \Omega$) at six different T_f using the formula

$$\langle m \rangle - M = \frac{1}{2}\left(1 + \frac{\varepsilon}{\Omega}\tanh\left(\frac{\Omega}{2k_B\sqrt{T_f^2 + T_0^2}}\right)\right) \qquad (2)$$

Three of the data sets and the corresponding fits are shown in Figure 3c. We find $\alpha = 0.145$ and $T_0 = 180$ mK, corresponding to $T_e = 182$ mK at the base temperature of the dilution refrigerator.

To determine t as a function of V_M, the extracted T_e and α are used to fit curves of the interdot charge transition. Figure 4 shows four such fits to the experimental data, with t as the sole free parameter. At small $|V_M|$, the increased tunnel coupling results in a clear broadening of the interdot charge transition, corresponding to increasingly large t.

The largest uncertainty in the values for t extracted by this method arises from the uncertainty in the determination of α and T_e. As described above, α and T_e were determined from fits to the thermally broadened curves based on the assumption $t = 0$ in the weak coupling limit. However, a good fit to those curves can be achieved with t as high as 6 μeV, resulting in an uncertainty of 3% in α and 12% in T_e. The corresponding effect on the uncertainty in t is significant for the smallest t, while for large t the uncertainty is very small.

We plot the resulting t as a function of V_M in the inset of Figure 4. The data are well fit by an exponential curve. Changing V_M by ~200 mV changes t by more than a factor of 10, corresponding to tuning the exchange interaction J by more than a factor of 100.[1] In analogy with predictions of oscillations in the exchange coupling between donors,[40] it is conceivable that t (and thus J) could oscillate as a function of V_M, due to the multiple valleys in Si. As shown in the inset to Figure 4, within the experimental uncertainty we observe no indication of such an oscillation in the tunnel coupling t as a function of V_M. This smooth behavior could indicate either an effectively smooth quantum well interface in the active region of the device,[41] as consistent with measurements of a large valley splitting in a QPC,[42] or it could be caused by valley relaxation in the presence of a rough interface.[43]

Another important characteristic of quantum dots is their charge stability and noise behavior. In Figure 2a−c, horizontal stripes of noise cut across the charging diagrams at several points. On the basis of their behavior as a function of the voltages on the gates defining the quantum dots and the QPC, we believe this noise is due to one or more charge traps beneath gate Q. As is clear from Figure 2, changing the voltage on gate L tunes the noise source in and out of resonance, and this behavior is consistent with previous reports that attributed some types of charge noise to the donor layer in semiconductor heterostructures.[44] Interestingly, this noise source seems to have little effect on the dots themselves. As can be seen in the figures, the lines corresponding to transitions in the quantum dot charge states pass through these noise stripes for the most part unchanged. The quantum dots themselves showed excellent long-term stability, with charge drift less than 0.03 e (which was the scan resolution) over a 7 day measurement period. This charge stability is consistent with other Si-based SETs which have shown drift of less than 0.01 e over a time period of weeks.[26]

In conclusion, we have demonstrated charge sensing measurements on a Si/SiGe quantum dot using an integrated quantum point contact. We have shown that the dot can be tuned into a single or double quantum dot. The device exhibited good charge stability, and the charge sensor measurements could resolve the interdot transition of a single electron at fixed total charge. Broadening of the interdot transition caused by charge delocalization at reduced $|V_M|$ was used to extract t, and the tunnel coupling was found to have an exponential dependence on this gate voltage. Control of t as a function of such a gate voltage is an important component in a number of approaches to quantum dot spin qubits.

Acknowledgment. We acknowledge useful discussions about quantum dot gate geometries with L. M. K. Vandersypen and C. M. Marcus. This work was supported in part by ARO and LPS (W911NF-08-1-0482), by NSF (DMR-0805045), by DOD, and by DOE (DE-FG02-03ER46028). The views and conclusions contained in this document are those of the authors and should not be interpreted as representing the official policies, either expressly or implied, of the U.S. Government. This research utilized NSF-supported shared facilities at the University of Wisconsin—Madison.

References

(1) Loss, D.; DiVincenzo, D. P. *Phys. Rev. A* **1998**, *57*, 120–126.
(2) Elzerman, J.; Hanson, R.; van Beveren, L.; Witkamp, B.; Vandersypen, L.; Kouwenhoven, L. *Nature* **2004**, *430*, 431–435.
(3) Petta, J. R.; Johnson, A. C.; Taylor, J. M.; Laird, E. A.; Yacoby, A.; Lukin, M. D.; Marcus, C. M.; Hanson, M. P.; Gossard, A. C. *Science* **2005**, *309*, 2180–2184.
(4) Johnson, A. C.; Petta, J. R.; Taylor, J. M.; Yacoby, A.; Lukin, M. D.; Marcus, C. M.; Hanson, M. P.; Gossard, A. *Nature* **2005**, *435*, 925–928.
(5) Koppens, F. H. L.; Buizert, C.; Tielrooij, K. J.; Vink, I. T.; Nowack, K. C.; Meunier, T.; Kouwenhoven, L. P.; Vandersypen, L. M. K. *Nature* **2006**, *442*, 766–771.
(6) Koppens, F. H. L.; Nowack, K. C.; Vandersypen, L. M. K. *Phys. Rev. Lett.* **2008**, *100*, 236802.
(7) Pioro-Ladrière, M.; Obata, T.; Tokura, Y.; Shin, Y.-S.; Kubo, T.; Yoshida, K.; Taniyama, T.; Tarucha, S. *Nat. Phys.* **2008**, *4*, 776.
(8) Reilly, D. J.; Taylor, J. M.; Petta, J. R.; Marcus, C. M.; Hanson, M. P.; Gossard, A. C. *Science* **2008**, *321*, 817.
(9) Khaetskii, A.; Loss, D.; Glazman, L. *Phys. Rev. B* **2003**, *67*, 195329.
(10) de Sousa, R.; Das Sarma, S. *Phys. Rev. B* **2003**, *68*, 115322.
(11) Yao, W.; Liu, R.-B.; Sham, L. J. *Phys. Rev. B* **2006**, *74*, 195301.
(12) Kane, B. *Nature* **1998**, *393*, 133–137.
(13) Vrijen, R.; Yablonovitch, E.; Wang, K.; Jiang, H. W.; Balandin, A.; Roychowdhury, V.; Mor, T.; Divincenzo, D. *Phys. Rev. A* **2000**, *62*, 012306.

(14) Friesen, M.; Rugheimer, P.; Savage, D. E.; Lagally, M. G.; van der Weide, D. W.; Joynt, R.; Eriksson, M. A. *Phys. Rev. B* **2003**, *67*, 121301.
(15) Morello, A.; Escott, C. C.; Huebl, H.; van Beveren, L. H. W.; Hollenberg, L. C. L.; Jamieson, D. N.; Dzurak, A. S.; Clark, R. G. Submitted for publication (arXiv:0904.1271).
(16) Slinker, K. A.; Lewis, K. L. M.; Haselby, C. C.; Goswami, S.; Klein, L. J.; Chu, J. O.; Coppersmith, S. N.; Joynt, R.; Blick, R. H.; Friesen, M.; Eriksson, M. A. *New J. Phys.* **2005**, *7*, 246.
(17) Sakr, M.; Jiang, H.; Yablonovitch, E.; Croke, E. *Appl. Phys. Lett.* **2005**, *87*, 223104.
(18) Berer, T.; Pachinger, D.; Pillwein, G.; Muhlberger, M.; Lichtenberger, H.; Brunthaler, G.; Schaffler, F. *Appl. Phys. Lett.* **2006**, *88*, 162112.
(19) Klein, L. J.; Savage, D. E.; Eriksson, M. A. *Appl. Phys. Lett.* **2007**, *90*, 033103.
(20) Simmons, C. B.; Thalakulam, M.; Shaji, N.; Klein, L. J.; Qin, H.; Blick, R. H.; Savage, D. E.; Lagally, M. G.; Coppersmith, S. N.; Eriksson, M. A. *Appl. Phys. Lett.* **2007**, *91*, 213103.
(21) Simmel, F.; Wharam, D. A.; Kastner, M. A.; Kotthaus, J. P. *Phys. Rev. B* **1999**, *59*, R10441–R10444.
(22) Rokhinson, L. P.; Guo, L. J.; Chou, S. Y.; Tsui, D. C. *Phys. Rev. B* **2001**, *63*, 035321.
(23) Fujiwara, A.; Inokawa, H.; Yamazaki, K.; Namatsu, H.; Takahashi, Y.; Zimmerman, N. M.; Martin, S. B. *Appl. Phys. Lett.* **2006**, *88*, 053121.
(24) Jones, G. M.; Hu, B. H.; Yang, C. H.; Yang, M. J.; Hajdaj, R.; Hehein, G. *Appl. Phys. Lett.* **2006**, *89*, 073106.
(25) Angus, S. J.; Ferguson, A. J.; Dzurak, A. S.; Clark, R. G. *Nano Lett.* **2007**, *7*, 2051–2055.
(26) Zimmerman, N. M.; Simonds, B. J.; Fujiwara, A.; Ono, Y.; Takahashi, Y.; Inokawa, H. *Appl. Phys. Lett.* **2007**, *90*, 033507.
(27) Liu, H. W.; Fujisawa, T.; Ono, Y.; Inokawa, H.; Fujiwara, A.; Takashina, K.; Hirayama, Y. *Phys. Rev. B* **2008**, *77*, 073310.
(28) Lansbergen, G. P.; Rahman, R.; Wellard, C. J.; Woo, I.; Caro, J.; Collaert, N.; Biesemans, S.; Klimeck, G.; Hollenberg, L. C. L.; Rogge, S. *Nat. Phys.* **2008**, *4*, 656–661.
(29) Nordberg, E. P.; Eyck, G. T.; Stalford, H.; Muller, R.; Young, R.; Eng, K.; Tracy, L.; Childs, K.; Wendt, J.; Grubbs, R.; Stevens, J.; Lilly, M. P.; Eriksson, M. A.; Carroll, M. S. Submitted for publication (arXiv:0906.3748).
(30) Zhong, Z.; Fang, Y.; Lu, W.; Lieber, C. M. *Nano Lett.* **2005**, *5*, 1143–1146.
(31) Hofheinz, M.; Jehl, X.; Sanquer, M.; Molas, G.; Vinet, M.; Deleonibus, S. *Appl. Phys. Lett.* **2006**, *89*, 143504.
(32) Hu, Y.; Churchill, H. O. H.; Reilly, D. J.; Xiang, J.; Lieber, C. M.; Marcus, C. M. *Nat. Nanotechnol.* **2007**, *2*, 622–625.
(33) Zwanenburg, F. A.; Rijmenam, C. E. W. M. V.; Fang, Y.; Lieber, C. M.; Kouwenhoven, L. P. *Nano Lett.* **2009**, *9*, 1071–1079.
(34) Fuhrer, A.; Füchsle, M.; Reusch, T. C. G.; Weber, B.; Simmons, M. Y. *Nano Lett.* **2009**, *9*, 707–710.
(35) Levy, J. *Phys. Rev. Lett.* **2002**, *89*, 147902.
(36) Divincenzo, D. P.; Bacon, D.; Kempe, J.; Burkard, G.; Whaley, K. B. *Nature* **2000**, *408*, 339.
(37) Dicarlo, L.; Lynch, H. J.; Johnson, A. C.; Childress, L. I.; Crockett, K.; Marcus, C. M. *Phys. Rev. Lett.* **2004**, *92*, 226801.
(38) Van Der Wiel, W. G.; Fujisawa, T.; Tarucha, S.; Kouwenhoven, L. P. *Rev. Mod. Phys.* **2002**, *75*, 1–22.
(39) Shaji, N.; Simmons, C. B.; Thalakulam, M.; Klein, L. J.; Qin, H.; Luo, H.; Savage, D. E.; Lagally, M. G.; Rimberg, A. J.; Joynt, R.; Friesen, M.; Blick, R. H.; Coppersmith, S. N.; Eriksson, M. A. *Nat. Phys.* **2008**, *4*, 540.
(40) Koiller, B.; Hu, X.; Das Sarma, S. *Phys. Rev. Lett.* **2001**, *88*, 027903.
(41) Friesen, M.; Eriksson, M. A.; Coppersmith, S. N. *Appl. Phys. Lett.* **2006**, *89*, 202106.
(42) Goswami, S.; Slinker, K. A.; Friesen, M.; McGuire, L. M.; Truitt, J. L.; Tahan, C.; Klein, L. J.; Chu, J. O.; Mooney, P. M.; van der Weide, D. W.; Joynt, R.; Coppersmith, S. N.; Eriksson, M. A. *Nat. Phys.* **2007**, *3*, 41–45.
(43) Friesen, M.; Coppersmith, S. N. Unpublished.
(44) Buizert, C.; Koppens, F. H. L.; Pioro-Ladrière, M.; Tranitz, H.-P.; Vink, I. T.; Tarucha, S.; Wegscheider, W.; Vandersypen, L. M. K. *Phys. Rev. Lett.* **2008**, *101*, 226603.

NL9014974